Applied Catalysis B: Environmental 325 (2023) 122340

Contents lists available at ScienceDirect

Applied Catalysis B: Environmental

journal homepage: www.elsevier.com/locate/apcatb

Photocatalytic partial oxidation of methane to carbon monoxide and hydrogen over CIGS solar cell

Chunyang Dong [a], Di Hu [a], Karima Ben Tayeb [b], Pardis Simon [c], Ahmed Addad [c], Martine Trentesaux [a], Danilo Oliveira de Souza [d], Sergei Chernyak [a], Deizi V. Peron [a], Amelle Rebai [e], Jean-Francois Guillemoles [e], Xavier Wallart [f], Bruno Grandidier [f], Andrei Y. Khodakov [a,*], Negar Naghavi [e,*], Vitaly V. Ordomsky [a,*]

[a] Univ. Lille, CNRS, Centrale Lille, ENSCL, Univ. Artois, UMR 8181 – UCCS – Unité de Catalyse et Chimie du Solide, F-59000 Lille, France
[b] Univ. Lille, CNRS, UMR 8516 – LASIRE – Laboratoire de Spectroscopie pour les Interactions, la Réactivité et l'Environnement, F-59000 Lille, France
[c] Univ. Lille, CNRS, INRAE, Centrale Lille, Univ. Artois, FR 2638-IMEC-Institut Michel-Eugène Chevreul, F-59000 Lille, France
[d] Elettra-Sincrotrone Trieste, Strada Statale 14 - km 163.5, 34149 Basovizza, Trieste, Italy
[e] CNRS, UMR 9006, Institut Photovoltaïque d'Ile-de-France (IPVF), 91120 Palaiseau, France,
[f] Univ. Lille, CNRS, Centrale Lille, Univ. Polytechnique Hauts-de-France, Junia-ISEN, UMR 8520 - IEMN, F-59000 Lille, France

ARTICLE INFO

Keywords:
CIGS
Methane
Oxidation
Syngas
Photocatalysis

ABSTRACT

Methane valorization is one of the main challenges in the modern chemical industry. However, existing processes require high reaction temperatures. The alternative photocatalytic routes for methane valorization at ambient conditions would be highly attractive. Today, photovoltaic (PV) generation of electricity is one of the main sources of renewable energy. PV absorbers could be excellent candidates for photochemical applications. Herein, we report selective methane photocatalytic oxidation at ambient conditions into CO and H_2 by conventional Cu(In,Ga)Se_2 (CIGS) absorbers used in solar cells. A thin film of CIGS coated over Mo exhibits exceptional performance in methane partial oxidation to CO and H_2 with a stable CO productivity of 2.4 mmol per gram of CIGS and a selectivity to CO of over 80%. The reaction proceeds via the facile dissociation of methane into disordered carbon and hydrogen over CIGS surface with subsequent regeneration of the surface by partial oxidation of carbon into CO.

1. Introduction

As the main constituent of renewable and fossil feedstocks (biogas, natural gas, shale gas…), methane is one of the most abundant carbonaceous feedstocks on earth. Currently methane is mostly used as fuel for heat and power generation, which coincides with a major emission of CO_2. Chemical valorization of methane into platform molecules is attractive from both economic and environmental aspects [1,2]. The main well-established reaction routes for methane transformation are steam reforming (SRM) or partial oxidation of methane (POM) into syngas (a mixture of CO and H_2) [3,4], which can be further used for the synthesis of methanol, olefins, middle distillates, acetic acid etc [5]. However, these processes require high temperature (700–1000 °C) due to the high stability of the methane molecule (C-H bond energy is 434 kJ·mol^{-1} (4.5 eV)) [6,7].

SRM: $CH_4 + 2\ H_2O = 4\ H_2 + CO_2$, $\Delta H^\circ = +206$ kJ/mol;

POM: $CH_4 + 1/2\ O_2 = 2\ H_2 + CO$, $\Delta H^\circ = -36$ kJ/mol;

Adopting solar energy as the driving force for methane activation can be one of the best strategies to address the above-mentioned energetic and environmental challenges [8–15]. Previously, it was shown that a combination of thermo-catalytic methane activation over metal-based catalysts such as CuRu [16], Rh [17–19], Pt [20], Ni [21] etc. with photocatalysis could reduce the SRM temperature. Nevertheless, a relatively high temperature (at least 300 °C) has been still required to achieve noticeable CH_4 conversion.

POM by molecular oxygen takes place at lower temperatures (500 – 700 °C) in comparison with thermal and photothermal processes of SRM

* Corresponding authors.
E-mail addresses: andrei.khodakov@univ-lille.fr (A.Y. Khodakov), negar.naghavi@chimieparistech.psl.eu (N. Naghavi), vitaly.ordomsky@univ-lille.fr (V.V. Ordomsky).

https://doi.org/10.1016/j.apcatb.2022.122340
Received 28 September 2022; Received in revised form 24 December 2022; Accepted 27 December 2022
Available online 2 January 2023

or DRM [4]. The main challenge of this process lies in the explosion risk of premixed CH_4/O_2 and undesirable over-oxidation route to the most stable oxidation products (H_2O and CO_2) [22–24]. Previously, we have shown that methane can be transformed into CO over a Zn-heteropoly-acid/TiO_2 photocatalyst at ambient temperature (**Table S1**) [25]. Though the CO selectivity reached over 84%, yet, only a trace amount of H_2 was detected. To date, to the best of our knowledge, direct production of syngas from methane partial oxidation at ambient temperature still has not been reported.

At the moment, the main rapidly growing technology for solar light utilization is photovoltaics (PV) which reached an energy generation of 1000 TWh in 2021 and has doubled since 2018 [26,27]. It solves the disadvantages of traditional bulk semiconductor photocatalysis due to the use of visible light, high quantum efficiency and scalable and adaptable technology. Among different PV technologies, $CuIn_xGa_{1-x}Se_2$ (CIGS) thin-film based solar cells are one of the most prominent [28,29]. The current state-of-the-art CIGS solar cells are based on p-n junctions, where 2 μm-thick p-type polycrystalline CIGS is directly co-evaporated onto a soda-lime glass substrate covered with molybdenum (Mo) back contact. The junction forms with a thin (≈ 30 nm) n-type CdS and i-ZnO/n-ZnO:Al front contact [30].

The CIGS-based solar cell has several important properties. First of all, it is a proven good photo-absorber with an extremely high solar cell efficiency of 23.3% [28,31]. CIGS can be produced at a reasonably low cost at industrial scale. Second, it has a high absorber coefficient in the visible range with a band gap that is tunable between 1.0 and 1.7 eV by changing the Ga/(Ga+In) ratio. Moreover, it presents higher stability compared to other emerging thin-film solar cell technologies [32]. Only a few articles have been published dealing with the use of CIGS for solar hydrogen production [33–35].

Herein, we report methane partial oxidation to syngas over CIGS absorbers at ambient conditions under light irradiation. Under an optimized condition, the CIGS thin film enables a stable synthesis of 3.4 mmol of CO, H_2 and CO_2 per gram of CIGS in 15 h with the CO/H_2 ratio at around 2:1 and the carbon-based CO selectivity over 80%. The reaction proceeds by sequential CH_4 dissociation and coupling into hydrocarbons followed by dehydrogenation into disordered carbon with further partial oxidation of carbon to CO (Fig. 1).

2. Experimental

2.1. Preparation of CIGS photocatalyst

The CIGS absorber layer was deposited in a co-evaporation reactor under high vacuum of 10^{-5} Pa on 800 nm DC sputtered Mo layer coated over soda lime glass. The four constituents (Cu, In, Ga and Se) were evaporated according to the standard 3-stage process. The substrate temperature was set to nominal values of T = 400 °C in the first stage and T = 425 °C in the 2nd and 3rd stage [36].

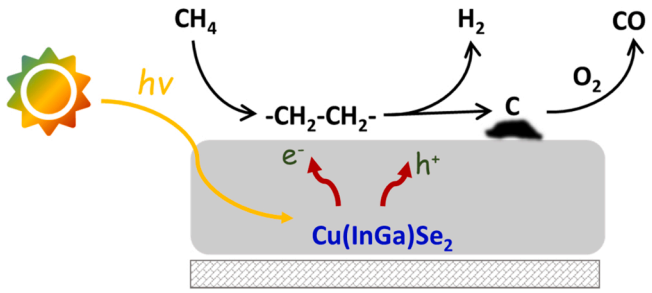

Fig. 1. Scheme of CH_4 partial oxidation to syngas over CIGS.

2.2. Characterization of CIGS photocatalyst

PL measurements were performed using a LabRam HR800-UV Horiba–Jobin Yvon spectrometer in combination with a confocal microscope, using a 532 nm excitation wavelength. Elemental in-depth composition profiles of the absorbers are obtained with glow discharge optical emission spectroscopy (GD-OES) using a GD-profiler HR by Horiba. Both EDX and scanning electron microscopy micrographs are obtained using a Zeiss Ultra 55 microscope. The crystalline structure of films was examined by X-ray diffraction (XRD) with a Panalytical Empyrean X-ray diffractometer using CuKα1 radiation (1.54057 Å) in the classical Bragg-Brentano θ-2θ configuration.

NAP XPS was performed at TEMPO-B beamline at the SOLEIL synchrotron facility in a setup previously described equipped with a NAP-XPS Phoibos 150 (SPECS GmbH) analyzer [37]. The sample holder was mounted vertically, with the sample normal aligned to the analyzer axis alongside a metallic gold foil. A spot light source (Hamamatsu L9588 LightningCure) was clamped to a quartz flange facing the sample for irradiation. The samples were exposed to CH_4 with or without irradiation, followed by subsequent oxidation under O_2 with or without irradiation. The gas was introduced into the analysis chamber by leak valves and evacuated via the analyzer nozzle. A steady-state regime was reached at the constant pressure of 1 mbar. Due to the overlapping of several Auger peaks, and the loss of photon flux at higher energy, the spectra were recorded at photon energy of 1100 eV and pass energy of 50 eV. The binding energy (BE) was calibrated with respect to the Au 4 f reference. Due to the difference in kinetic energies (KE), only a relative ratio between intensities could be determined.

The in-situ X-ray absorption spectra were recorded at the XAFS beamline station of the Elettra Synchrotron (Trieste, Italy) [38]. The beam was vertically collimated using silicon ingot with Pt-coating mirror positioned at 3.0 mrad with respect to the direct beam. No noticeable features on the XAFS signal by the Pt coating, particularly, L edges of Pt (11.5–14 keV) were detected on experimental spectra. The beam was monochromatized by a fixed-exit double cam double crystal monochromator, using a pair of Si (111) crystals. Harmonic rejection for Cu K-edge is achieved by detuning slightly Si (111) crystal. The monochromatic beam is 1.2 mm vertically and horizontally variable according to the sample size inside the capillary. Prior to the XAS measurements, the CIGS powder scratched from the surface of the plate was packed between two layers of quartz wool within a quartz capillary (O.D. = 2 mm). Next, the capillary was stabilized on a metallic holder (with epoxy glue) and connected to the gas lines of N_2, CH_4 and air. During the test, the spectra (using in transmission mode) of the catalysts were recorded via the following steps: (1) 30 min in dark under 4 bar N_2; (2) 60 min illuminated by a spot light source (Hamamatsu L9588 LightningCure) in 4 bar CH_4, N_2 or air.

Ultraviolet (UV) photoemission spectroscopy was performed with a helium UV lamp which produces spectral lines of $h\nu$ = 21.22 eV (He I) and 40.82 eV (He II). The energy scale of the spectrometer was calibrated using the Au 4 $f_{7/2}$ core level at 84.0 eV of a clean and sputtered Au sample. For the spectra acquisition, the bias applied to the sample was either zero or − 3 V to get a clear signal of the secondary electron cutoff.

The analysis of paramagnetic species has been performed by Continuous-Wave - Electron Paramagnetic Resonance (CW–EPR). These experiments were performed on a Bruker ELEXSYS E500 spectrometer operating in X-band (9.5 GHz). The experimental conditions for recording spectra are a microwave power of 10 mW, modulation amplitude of 2 G, corresponding to non-saturation conditions. The solid state EPR spectra were recorded at 100 K. The aqueous phase spin trapping EPR experiments are performed at room temperature with [DMPO] = 80 mM, microwave power of 10 mW, modulation amplitude of 0.2 G, a conversion time of 5 ms and 100 scans. An EPR quick pressure tube is used to work under CH_4 (5 bar) atmosphere. A spot light source (Hamamatsu L9588 LightningCure) was used for the illumination. Data

were simulated using WinSim software.

In-situ diffuse reflectance infrared Fourier transform (DRIFT) spectra were recorded on a Nicolet 6700 FT-IR Spectrometer (Thermo Fisher Scientific) with a mercury cadmium telluride detector using a Praying Mantis DRIFT cell from Harrick. Before the analysis, a piece of CIGS plate was transferred into the in-situ reaction cell and was purged by a continuous CH_4 flow (10 mL/min) at atmospheric pressure for 30 min. Afterwards, a spectrum was recorded as the background. Subsequently, the CIGS plate was irradiated by a spotlight source (Hamamatsu L9588 LightningCure) for 30 min. During the irradiation process, the DRIFT spectrum was recorded continuously (32 scans at a resolution of 4 cm^{-1}).

2.3. Photocatalytic evaluation measurement

The photocatalytic reactions were performed in a 250 mL batch reactor, with a mercury-xenon (Hg-Xe) arc lamp (Newport, 200 – 500 W) used as a light source. A quartz window is located on the top of the reactor which enables the vertical transmission of the incident light. The temperature of reactor was maintained at 20 °C by a circulating water machine. After photocatalytic reactions, the gaseous products were analyzed by a gas chromatograph (PerkinElmer Clarus 580 GC) equipped with a PoraBOND Q and a ShinCarbon ST 100/120 columns, as well as a thermal conductive detector and a flame ionized detector.

3. Results and discussion

3.1. Structure and catalytic performance of CIGS

A 2 μm thick CIGS absorber was deposited on the Mo-coated soda-lime glass substrates employing the three-stage co-evaporation processes [39]. The surface morphology and cross-sections of the CIGS absorbers investigated by scanning electron microscopy (SEM) are shown in Fig. 2 and **Figure S1, SI**. The surface of the films is quite rough (Fig. 2), however, the films are dense and the grains are well defined.

The X-ray fluorescence analysis showed an average ratio of 0.8 for Cu/(Ga+In) (CGI) and 0.3 for [Ga]/([Ga]+[In]) (GGI). **Figure S2, SI** shows in-depth profiles of Ga ([Ga]/([Ga]+[In]) measured by glow discharge optical emission spectroscopy (GD-OES). Owing to a preferred reaction of In with Cu over Ga with Cu during film growth, the three-stage deposition results always in a double-graded composition profile with a higher Ga content towards the back and the front of the film, and a characteristic notch of low Ga content in between. These samples present a Ga/(Ga+In) (GGI) ≈ 0.43 at the front interface and a GGI ≈ 0.6 at the back. The XRD pattern of the CIGS absorber (Fig. 2**b)** shows the presence of CIGS phases and Mo back contact [40]. Typical (112), (220/204) and (312/316) planes of CIGS thin-film are observed at 2θ = 27.2°, 45.0° and 52.8°, respectively, while the (110) Mo layer is observed at 40.5°. Based on the literature, such CIGS absorbers exhibit a chalcopyrite structure with a preferred (112) orientation. The photoluminescence (PL) spectrum of CIGS absorber measured at room temperature using a 532 nm excitation wavelength (2.33 eV) presents a typical broad single peak corresponding to the energy transition at around 1.16 eV (**Figure S3, SI**).

Photocatalytic oxidation of methane was investigated on the glass/Mo/CIGS sample of = 2 × 2 cm^2 containing 2 mg of CIGS (Fig. 2). The 250 mL reactor has been filled with air and methane with subsequent light irradiation using a 400 W Hg-Xe lamp. The pressure ratio between air and methane was varied from 0.1/ 9.9–1/9 (unit, bar), outside of the explosive range of methane. The products including CO, H_2, CO_2 and a small amount of C_2H_6 were detected during photocatalytic reactions. Note that no products have been detected using visible light irradiation (**Table S2, SI**)

The thermocatalytic partial oxidation of methane to syngas is challenging because it is difficult to control the reaction selectivity to CO and to avoid full oxidation to CO_2 at relatively low temperatures (400 – 500 °C) [41]. Temperature and partial pressures of methane and oxygen are the key parameters for the selectivity control. In our case, the reaction is performed at room temperature over CIGS and the varied parameter was the pressures of methane and oxygen. The lowest air

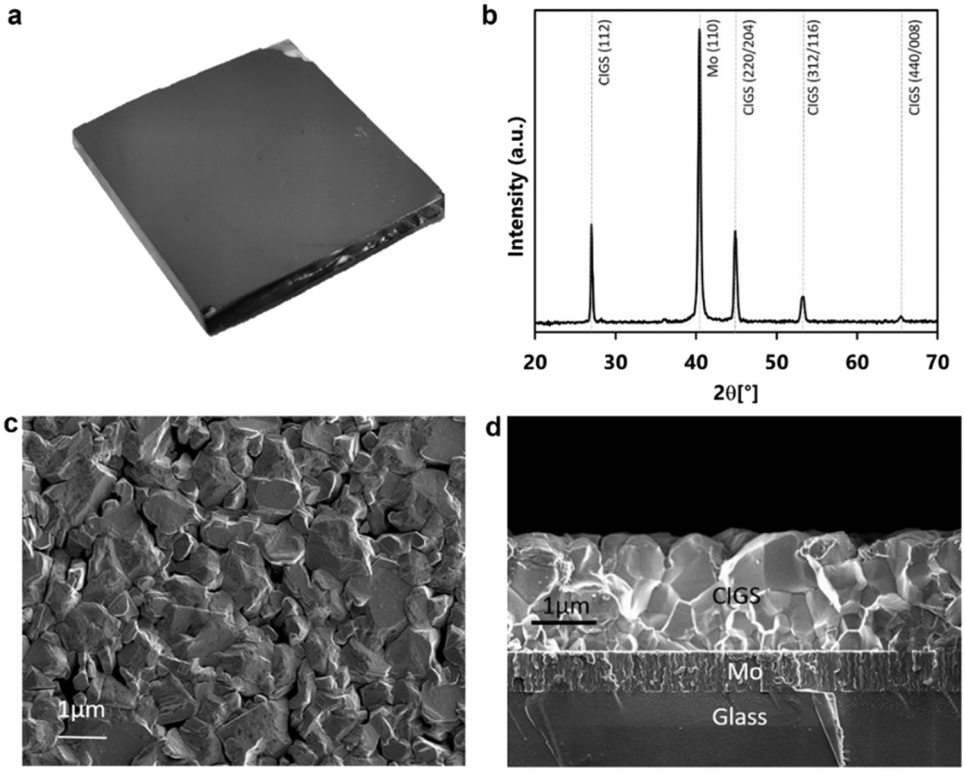

Fig. 2. (a) Image of CIGS coated plate 2 × 2 cm^2, (b) XRD pattern of CIGS, SEM analysis of CIGS layer coating: (c) top view and (d) cross-section.

content (air/methane = 0.1/9.9) results in a generation of 0.5 mmol/g of CO with a carbon-based selectivity of about 70% (Fig. 3**a**). An increase in air pressure to 0.25 bar results in a sharp increase in the CO production to 1.7 mmol/g with the same selectivity. The CO/H_2 ratio under this condition is around 2:1. Higher air content results in the suppression of catalytic activity, which coincides with an increase in the CO_2 selectivity.

Further, the stability of the catalyst at optimal conditions of air/methane = 0.25/9.75 (bar) has been studied by performing 5 cycles (Fig. 3**b**). After each cycle, the reactor was evacuated and charged with fresh reactants without any regeneration treatment. It is interesting to note that the CO production and carbon-based CO selectivity even increase after the first catalytic cycle, reaching 2.4 mmol/g and 80%, respectively, at the CO/H_2 ratio of about 2:1 with a stable performance afterward. This fact could be explained by the deactivation of non-selective sites after the first reaction cycle.

3.2. *Mechanism of the reaction*

Probing the evolution of the oxidation state of the elements in CIGS during the reaction is critical for understanding the mechanism of photocatalytic partial oxidation of methane. Consequently, the in-situ X-ray absorption spectroscopy studies of CIGS plate at Cu, Ga and Se K-edges were conducted during CH_4 and O_2 treatments. The X-ray absorption near edge spectra (XANES) of Ga and Se K-edges did not show any noticeable change (**Figure S4-S5, SI**). Conversely, the intensity of the white line of Cu K-edge XANES which corresponds to Cu^+ slightly decreases during the catalyst treatment in CH_4 with a subsequent increase during O_2 treatment under light irradiation (Fig. 4**a**). The decrease in the intensity of the Cu K-edge white line suggests some increase in the electronic density of Cu cations during the interaction with methane. The subtraction of the initial spectrum shows the appearance of a negative peak at 8985 and 8992 eV (Fig. 4**b**) during treatment in the methane and CH_4/O_2 atmosphere. This feature has been assigned earlier to a decrease in electron density, for example, by the interaction of metal with adsorbed molecules such as CO or O_2 [42,43]. Additional cycles confirm that the process is reversible. The state of Cu could be recovered by exposure to air to the initial level. Note that coordination of Cu does not evolve during the reaction.

The CIGS sample was further characterized by synchrotron-based near ambient pressure X-ray photoemission spectroscopy (NAP-XPS) (Fig. 5). In the fresh sample, the Cu $2p_{3/2}$, In $3d_{5/2}$ and Se $3d_{5/2}$ BEs are locate at 932.1 eV, 444.6 eV and 54.1 eV, which corresponds to the oxidation states of Cu^+, In^{3+} and Se^{2-}, respectively [44,45], along with the modified Auger parameter equal to 1849.6 eV as well as the Cu $L_2{}_3M_{4,5}M_{4,5}$ Auger peak shape. These XPS and Auger data are characteristic of the CIGS material [46,47]. All BEs values are summarized in **Table S3, SI**.

The exposure to CH_4 under irradiation does not result in any spectral shift of Se 3d, In 3d and Cu $L_{2,3}M_{4,5}M_{4,5}$ spectra. However, the intensity of the carbon peak on the survey spectra is highly increased. The exposure to methane also leads to a drastic loss in the intensity in the Cu 2p spectra and In 3d spectra recorded with low kinetic energy (Fig. 5**a**). Note that the Cu 2p photoelectrons are superficial. The exposure to methane under irradiation leads to the deposition of carbon on the surface of CIGS plate, thus to a drastic loss in the intensity in the Cu 2p spectra due to their low kinetic energy (**Figure S6, SI**). In contrast, Cu Auger peak has a 918 eV kinetic energy, the intensity, thus, remains high enough when the CIGS is exposed to CH_4. The removal of carbon deposited on the CIGS surface by O_2 treatment results in the increase in the intensity of Cu 2p XPS peak.

The carbon to indium ratio is multiplied by a factor of 35.8 (**Table S3, SI**) after exposure to methane under irradiation. This is consistent with the deposition of carbon on the surface of the sample. Carbon deposition on the CIGS surface can also lead to higher electronic density over Cu and thus a decrease in the intensity of Cu K-edge white line observed in the XAS spectra (Fig. 4). Moreover, the Se species of CIGS demonstrated good stability under irradiation. The peak position and the ratio between Se $3d_{5/2}$ and Se $3d_{3/2}$ suggest that the valence state of Se was not modified when exposed to CH_4 or O_2 upon illumination (**Figure S7, SI**).

After subsequent exposure to O_2 under irradiation, Son the survey spectra is highlye 3d, In 3d and Cu $L_{2,3}M_{4,5}M_{4,5}$ spectra restored their initial state, whereas the carbon to indium ratio decreases to its original value (Fig. 5 **and Table S3, SI**). At the same time, the intensity of Cu 2p spectra partially recovered. The C 1s spectra also show additional peaks at higher BEs that can be attributed to oxygenated carbon species.

In order to confirm the deposition of carbon on the surface of CIGS, we have performed SEM analysis of the plate treated with CH_4 under irradiation. Fig. 6 demonstrates the presence of the non-uniformly distributed carbon coating after this treatment. The formation of this carbon coating coincided with a generation of 350 $\mu mol_{H2}/g$. The Raman spectra also demonstrate the appearance of a broad peak with a maximum at 1400 cm^{-1} with a shoulder at 1550 cm^{-1} after treatment of CIGS by methane. According to the literature, carbon materials usually show the in-phase vibration of the graphite lattice (G band) at about 1575 cm^{-1} related to sp^2 bonds of carbon and a disorder band caused by the graphite edges with sp^3 configuration (D band) at approximately 1355 cm^{-1} [48]. Taking it into account, the carbon deposited over CIGS demonstrates a highly disordered structure with a low contribution of

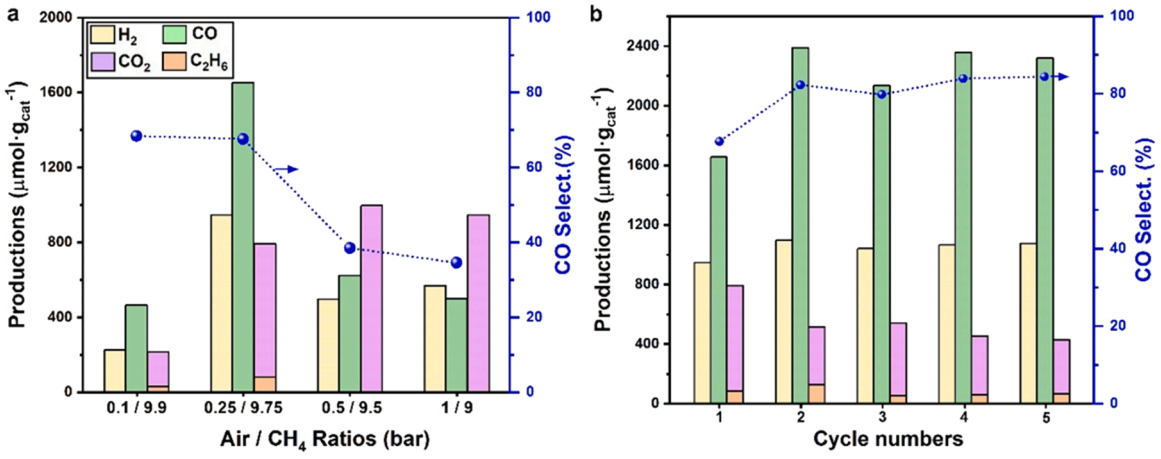

Fig. 3. (a) Photocatalytic performance of CIGS sample under different air/CH_4 ratios. (b) Stability test of CIGS samples in 5 cyclic tests. Reaction conditions: 2 mg catalyst, 250 mL reactor, 20 °C, 15 h, a 400 W Hg-Xe lamp as the light source.

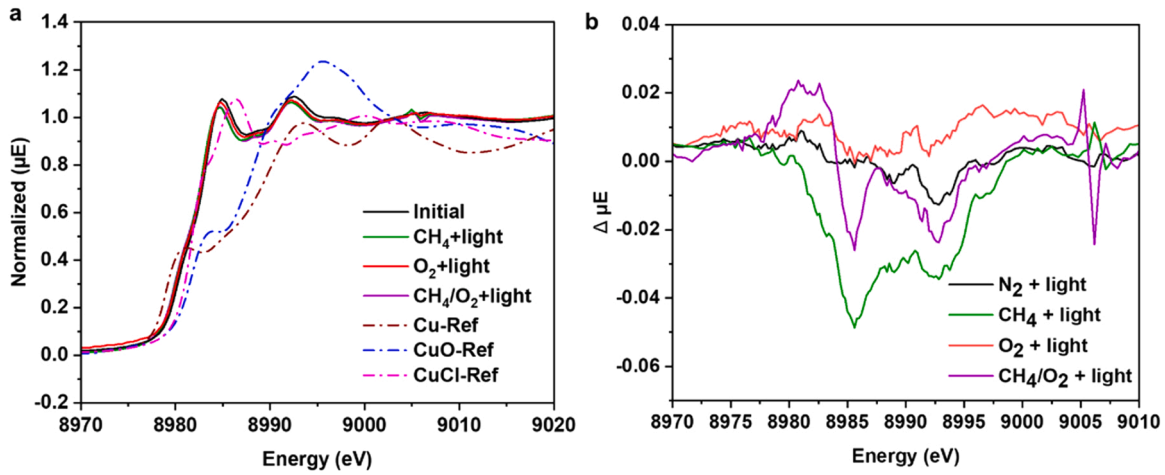

Fig. 4. In-situ Cu K-edge XANES spectra of CIGS after N_2, CH_4, O_2 and CH_4/O_2 treatment in comparison with reference samples (a) and the difference between these samples and initial spectrum (b).

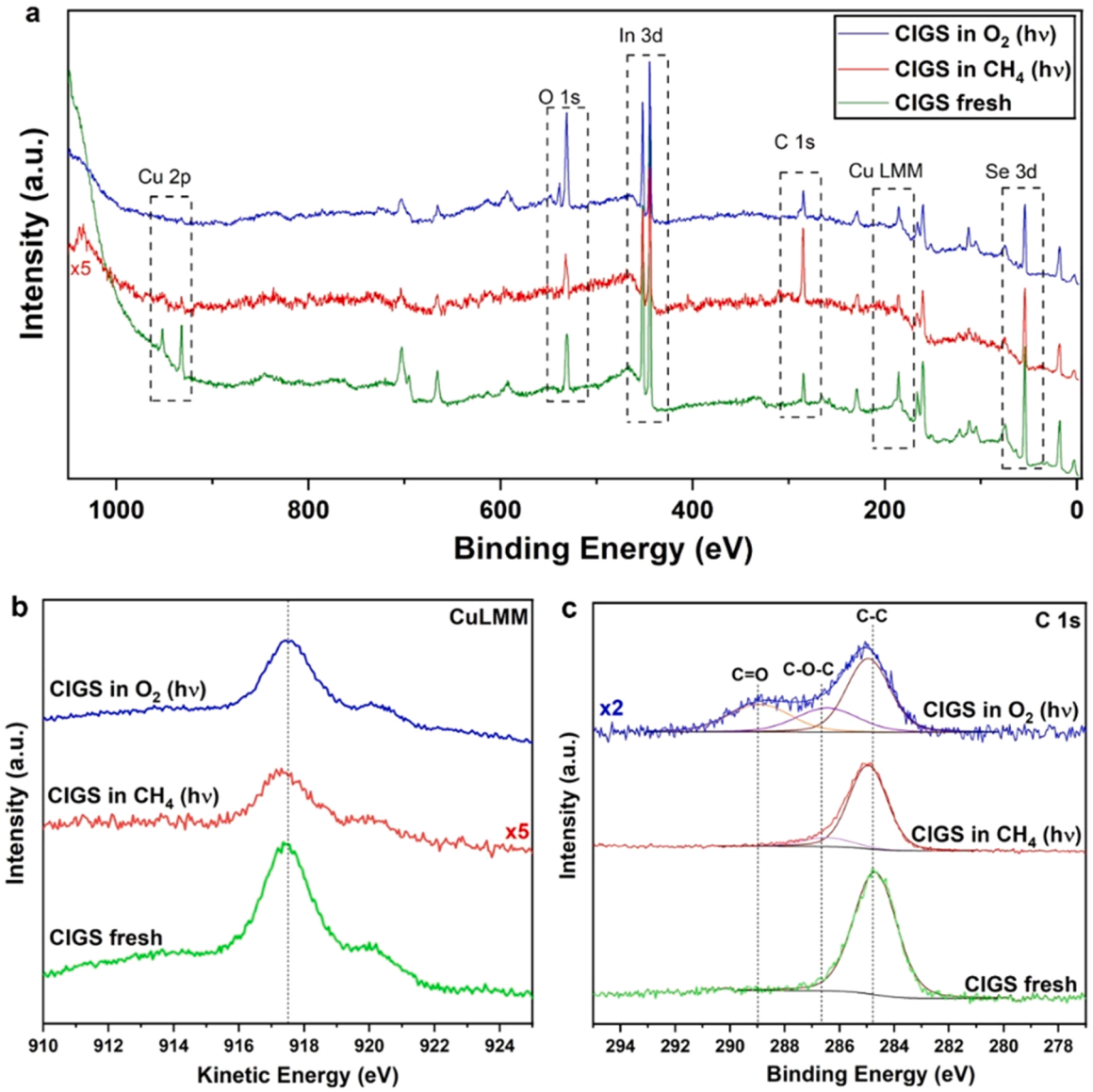

Fig. 5. In-situ XPS normalized spectra of CIGS under different conditions (a) survey spectra; (b) Cu $L_{2,3}M_{4,5}M_{4,5}$ spectra; (c) C 1s spectra.

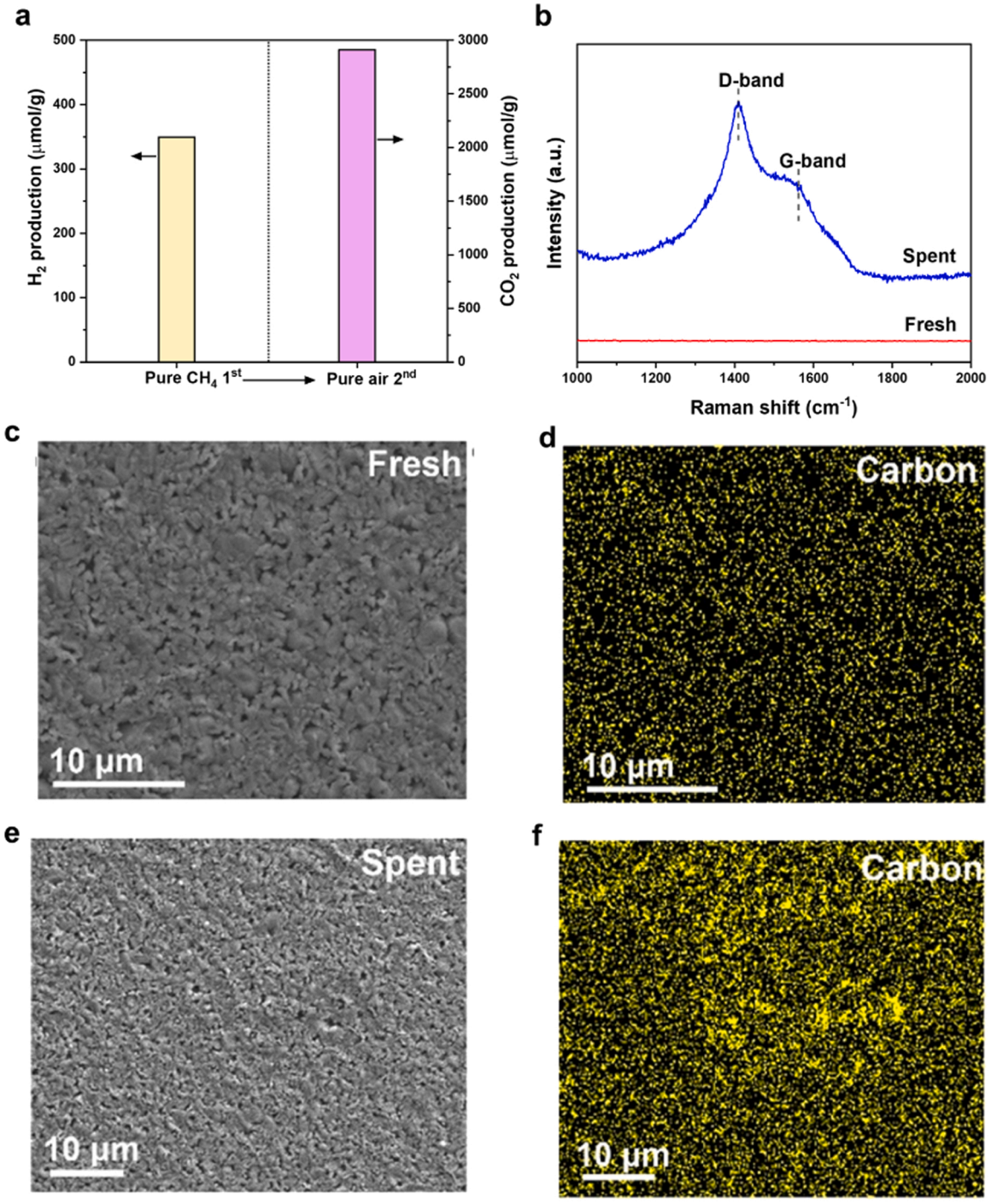

Fig. 6. (a) Photocatalytic performance of CIGS plate under sequential pure CH_4 and air conditions. Reaction condition: 2 mg catalyst, 20 °C, 5 bar, 15 h irradiation. (b) Raman spectra of fresh and spent CIGS plate. SEM and EDX-mapping images of carbon over fresh (c,d) and spent CIGS plate (e,f). Note that the spent CIGS plate underwent the same treatment in pure CH_4 atmosphere as mentioned above.

ordered graphite sheet.

Subsequent irradiation of the plate in the presence of air results in the oxidation of carbon, which coincides with a production of carbon dioxide (2900 $\mu mol_{CO2}/g$). The generation of CO_2 on exposure to air of CIGS plate pretreated with methane under irradiation further confirms the deposition of carbon.

To gain more insight into the reaction mechanism, we performed in-situ electron paramagnetic resonance (EPR) studies on a CIGS sample with 5,5-dimethyl-1-pyrroline N-oxide (DMPO) as a radical trapping agent within aqueous media. Apparently, upon light irradiation, no methyl radicals ($\cdot CH_3$) but only hydroxyl radicals ($\cdot OH$) were observed in CH_4 atmosphere (**Figure S8, SI**). Besides, the intensity of $\cdot OH$ signal in CH_4 is quite weak compared to that in air atmosphere. Therefore, it is not likely that $\cdot CH_3$ is an intermediate in the methane activation process. It seems that methane dissociation results in simultaneous splitting of several C-H bonds. Subsequently, we investigated the evolution of surface intermediates on CIGS plate using in-situ diffuse reflectance infrared Fourier transform (DRIFT) spectroscopy. A broad absorption band centered at 2850 cm^{-1} was observed and continuously increased upon irradiation in the flow of methane (**Figure S9, SI**). According to the

literature, this signal can be assigned to the symmetric stretching vibrations of CH_2 groups [49]. Taking into account the detection of C_2H_6 as a minor side product during photocatalysis (in the presence of both CH_4 and air) (Fig. 3), the surface hydrocarbon species generated by methane activation by photo-generated holes should be intermediates prior to the formation of disordered carbon. The low ratio of H_2 to CO_2 (Fig. 6) and the variation of O 1s peak in NAP-XPS (Fig. 5) at sequential CH_4 and air treatment suggest oxygen-assisted activation of methane over the surface of CIGS.

The dissociation of methane over a CIGS cell could proceed through interaction with paramagnetic species . The solid state EPR analysis of CIGS shows the signals which can be assigned to Mo^{5+} produced due to partial oxidation of Mo to oxide or selenide and conducting electrons with hyperfine couplings between the two isotopes Ga^{69} and Ga^{71} (**Figure S10, SI**). However, the signals do not demonstrate reversible character with on-off light switching, which excludes their role in catalysis.

Ultraviolet photoelectron spectroscopy (UPS) analysis has been used to identify the states in the valence band. The spectra (Fig. 7**a**) were recorded by He II (40.82 eV) radiation for a fresh CIGS sample before and after Ar^+-ion etching of the surface. The edge of the valence band E_V is found 0.4 eV below the Fermi level. A shoulder in the valence band, which becomes more pronounced upon etching the CIGS surface, is measured about 3.0 eV below the Fermi level. This shoulder is consistent with a peak of the density of states related to the Cu 3*d* orbitals [50,51]. In contrast to the visible light spectrum where photons have energies lower than ~3 eV, a value corresponding to the energy separation between these states and the conduction band of CIGS corresponds to UV irradiation. The Hg-Xe lamp, which emits UV light, can generate electron-hole pairs from these bands under irradiation. Due to the high density of Cu 3*d*-like states, a significant concentration of photoexcited holes is available at the CIGS surface. As their energy is well below the valence band, they have an oxidizing power higher than 1.75 eV. Therefore, they can react with CH_4 molecules over copper sites, as indicated by the drop of the Cu 2p peak in NAP XPS upon reaction (Fig. 5) and Cu K-edge in XAS (Fig. 4), leading to the production of hydrocarbon species with further dehydrogenation to carbon and hydrogen (Fig. 7**b**).

Overall, based on all the experimental results, the mechanism of partial oxidation of methane over CIGS can involve methane dissociation, coupling and further dehydrogenation on the surface of CIGS with the generation of hydrogen and carbon (Fig. 1). Subsequent oxidation of carbon on the surface of CIGS results in the generation of CO with partial oxidation of hydrogen to water. It is interesting to note that in comparison with traditional photocatalytic methane activation, it does not lead to the generation of ethane (**Table S1, SI**). It could be explained by deep C-H dissociation of methane to carbon with strong adsorption on the surface in comparison with conventional catalysts generating $\cdot CH_3$ radicals [10].

Traditionally, the mechanism of thermo-catalytic partial oxidation of methane implies several steps. It starts with deep oxidation to CO_2 and H_2O with subsequent SRM and DRM to CO and H_2 [52,53]. Thermocatalytic DRM requires high temperatures for CO_2 conversion to syngas and it makes difficult low temperature reforming and partial oxidation of methane. The proposed photocatalytic route using PV technology proposes an alternative mechanism by methane splitting into hydrogen and carbon with subsequent oxidation to CO.

4. Conclusion

In summary, we demonstrated that thin film CIGS absorbers exhibited noticeable catalytic activity in methane activation and could be used for the selective partial oxidation of methane to syngas at ambient temperature. The mechanism of the reaction involves the dissociation of CH_4 on the surface of CIGS with subsequent coupling, dehydrogenation and oxidation of carbon to CO. Our study provides a fresh insight into the use of photovoltaic absorbers for catalytic applications and opens broad perspectives for the industrial valorization of solar cells in catalysis.

CRediT authorship contribution statement

Chunyang Dong: Investigation, Writing – original draft, Data analysis; **Andrei Y. Khodakov, Negar Naghavi and Vitaly V. Ordomsky:** Supervision, Writing – review & editing, Funding acquisition, Project administration; **Di Hu:** Investigation; **Karima Ben Tayeb:** Investigation, Data analysis; **Pardis Simon:** Investigation, Data analysis, Writing; **Ahmed Addad:** Investigation; **Martine Trentesaux:** Investigation; **Danilo Oliveira de Souzad:** Investigation, Data curation; **Sergei Chernyak:** Investigation; **Deizi V. Peron:** Investigation; **Amelle Rebai:** Investigation; **Jean-Francois Guillemoles:** Methodology; **Xavier Wallart:** Investigation, Data analysis; **Bruno Grandidier:** Investigation, Writing.

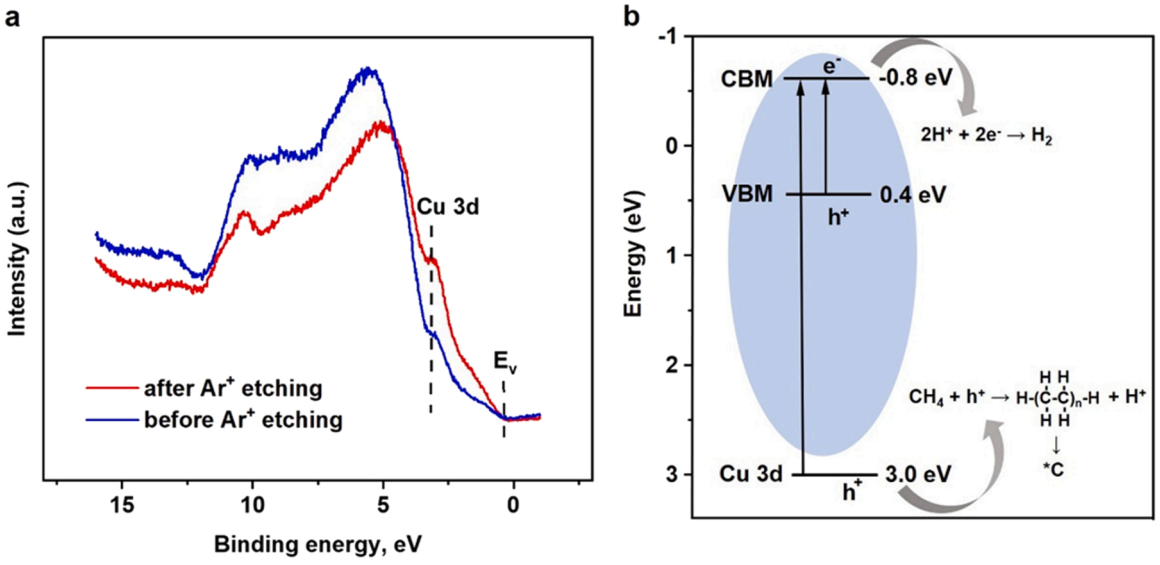

Fig. 7. (a) UPS spectra acquired for an as-grown CIGS sample and after Ar^+ treatment for 10 min at an energy of 1 keV. The positions of the Cu 3d like-states and the Fermi level are indicated with vertical segments. (b) Band levels and elementary steps in methane coupling.

Declaration of Competing Interest

The authors declare that they have no known competing financial interests or personal relationships that could have appeared to influence the work reported in this paper.

Data availability

Data will be made available on request.

Acknowledgments

The authors gratefully acknowledge the support of the French National Research Agency (SolarMethaCell project). We are grateful to the Elettra and Soleil synchrotrons for the use of beamtime.

Author contributions

C.D., V.V.O., N.N. and A.Y.K. conceived the idea for this work. All authors contributed to the design of the experimental setup and experimental procedures. A.R., J-F.G. and N.N. prepared and characterized the material. C.D. and D.H. performed photocatalytic tests. P.S., M.T., C. D., D.V.P. and S.C. performed in-situ XAFS and XPS measurements and analysis. A.A. performed the SEM analysis. K.B.M. characterized the catalysts and reaction intermediates using EPR. C.D., A.Y. and V.V.O. wrote the draft and all authors took part in improving the manuscript.

Additional information

Supplementary Information is available for this paper.

Appendix A. Supporting information

Supplementary data associated with this article can be found in the online version at doi:10.1016/j.apcatb.2022.122340.

References

[1] P. Tang, Q. Zhu, Z. Wu, D. Ma, Methane activation: the past and future, Energy Environ. Sci. 7 (2014) 2580–2591.
[2] W. Taifan, J. Baltrusaitis, CH4 conversion to value added products: potential, limitations and extensions of a single step heterogeneous catalysis, Appl. Catal. B: Environ. 198 (2016) 525–547.
[3] H. Zhang, Z. Sun, Y.H. Hu, Steam reforming of methane: current states of catalyst design and process upgrading, Renew. Sustain. Energy Rev. 149 (2021), 111330.
[4] B. Christian Enger, R. Lødeng, A. Holmen, A review of catalytic partial oxidation of methane to synthesis gas with emphasis on reaction mechanisms over transition metal catalysts, Appl. Catal. A: Gen. 346 (2008) 1–27.
[5] V.V. Ordomsky, Y. Luo, B. Gu, A. Carvalho, P.A. Chernavskii, K. Cheng, A. Y. Khodakov, Soldering of Iron Catalysts for Direct Synthesis of Light Olefins from Syngas under Mild Reaction Conditions, ACS Catal. 7 (2017) 6445–6452.
[6] J.P. Van Hook, Methane-steam reforming, Catal. Rev. 21 (1980) 1–51.
[7] A.H. Elbadawi, L. Ge, Z. Li, S. Liu, S. Wang, Z. Zhu, Catalytic partial oxidation of methane to syngas: review of perovskite catalysts and membrane reactors, Catal. Rev. 63 (2021) 1–67.
[8] H. Song, X. Meng, Z.-J. Wang, H. Liu, J. Ye, Solar-energy-mediated methane conversion, Joule 3 (2019) 1606–1636.
[9] X. Li, C. Wang, J. Tang, Methane transformation by photocatalysis, Nat. Rev. Mater. 7 (2022) 617–632.
[10] D. Hu, V.V. Ordomsky, A.Y. Khodakov, Major routes in the photocatalytic methane conversion into chemicals and fuels under mild conditions, Appl. Catal. B: Environ. 286 (2021), 119913.
[11] X. Yu, V.L. Zholobenko, S. Moldovan, D. Hu, D. Wu, V.V. Ordomsky, A. Y. Khodakov, Stoichiometric methane conversion to ethane using photochemical looping at ambient temperature, Nat. Energy 5 (2020) 511–519.
[12] J. Ma, Q. Zhang, Z. Chen, K. Kang, L. Pan, S. Wu, C. Chen, Z. Wu, J. Zhang, L. Wang, Design of frustrated Lewis pair in defective TiO2 for photocatalytic non-oxidative methane coupling, Chem. Catal. (2022).
[13] S. Wu, X. Tan, J. Lei, H. Chen, L. Wang, J. Zhang, Ga-doped and Pt-loaded porous TiO_2–SiO_2 for photocatalytic nonoxidative coupling of methane, J. Am. Chem. Soc. 141 (2019) 6592–6600.
[14] Z. Chen, S. Wu, J. Ma, S. Mine, T. Toyao, M. Matsuoka, L. Wang, J. Zhang, Non-oxidative coupling of methane: N-type doping of niobium single atoms in TiO_2–SiO_2 induces electron localization, Angew. Chem. Int Ed. Engl. 60 (2021) 2–11.
[15] W. Zhang, C. Fu, J. Low, D. Duan, J. Ma, W. Jiang, Y. Chen, H. Liu, Z. Qi, R. Long, Y. Yao, X. Li, H. Zhang, Z. Liu, J. Yang, Z. Zou, Y. Xiong, High-performance photocatalytic nonoxidative conversion of methane to ethane and hydrogen by heteroatoms-engineered TiO_2, Nat. Commun. 13 (2022) 2806.
[16] L. Zhou, J.M.P. Martirez, J. Finzel, C. Zhang, D.F. Swearer, S. Tian, H. Robatjazi, M. Lou, L. Dong, L. Henderson, P. Christopher, E.A. Carter, P. Nordlander, N. J. Halas, Light-driven methane dry reforming with single atomic site antenna-reactor plasmonic photocatalysts, Nat. Energy 5 (2020) 61–70.
[17] S. Shoji, X. Peng, A. Yamaguchi, R. Watanabe, C. Fukuhara, Y. Cho, T. Yamamoto, S. Matsumura, M.-W. Yu, S. Ishii, T. Fujita, H. Abe, M. Miyauchi, Photocatalytic uphill conversion of natural gas beyond the limitation of thermal reaction systems, Nat. Catal. 3 (2020) 148–153.
[18] D. Takami, A. Yamamoto, H. Yoshida, Dry reforming of methane over alumina-supported rhodium catalysts at low temperatures under visible and near-infrared light, Catal. Sci. Technol. 10 (2020) 5811–5814.
[19] H. Song, X. Meng, Z.-J. Wang, Z. Wang, H. Chen, Y. Weng, F. Ichihara, M. Oshikiri, T. Kako, J. Ye, Visible-light-mediated methane activation for steam methane reforming under mild conditions: a case study of Rh/TiO2 catalysts, ACS Catal. 8 (2018) 7556–7565.
[20] F. Pan, X. Xiang, W. Deng, H. Zhao, X. Feng, Y. Li, A novel photo-thermochemical approach for enhanced carbon dioxide reforming of methane, ChemCatChem 10 (2018) 940–945.
[21] Z. Rao, Y. Cao, Z. Huang, Z. Yin, W. Wan, M. Ma, Y. Wu, J. Wang, G. Yang, Y. Cui, Z. Gong, Y. Zhou, Insights into the nonthermal effects of light in dry reforming of methane to enhance the H2/CO ratio near unity over Ni/Ga2O3, ACS Catal. 11 (2021) 4730–4738.
[22] S.J. Freakley, N. Dimitratos, D.J. Willock, S.H. Taylor, C.J. Kiely, G.J. Hutchings, Methane oxidation to methanol in water, Acc. Chem. Res. 54 (2021) 2614–2623.
[23] F. Wang, W.-Z. Li, J.-D. Lin, Z.-Q. Chen, Y. Wang, Crucial support effect on the durability of Pt/MgAl2O4 for partial oxidation of methane to syngas, Appl. Catal. B: Environ. 231 (2018) 292–298.
[24] D. Zeng, Y. Qiu, M. Li, L. Ma, D. Cui, S. Zhang, R. Xiao, Spatially controlled oxygen storage materials improved the syngas selectivity on chemical looping methane conversion, Appl. Catal. B: Environ. 281 (2021), 119472.
[25] X. Yu, V. De Waele, A. Löfberg, V. Ordomsky, A.Y. Khodakov, Selective photocatalytic conversion of methane into carbon monoxide over zinc-heteropolyacid-titania nanocomposites, Nat. Commun. 10 (2019) 700.
[26] P.K. Nayak, S. Mahesh, H.J. Snaith, D. Cahen, Photovoltaic solar cell technologies: analysing the state of the art, Nature Reviews, Materials 4 (2019) 269–285.
[27] B. Parida, S. Iniyan, R. Goic, A review of solar photovoltaic technologies, Renew. Sustain. Energy Rev. 15 (2011) 1625–1636.
[28] N. Mufti, T. Amrillah, A. Taufiq, Sunaryono Aripriharta, M. Diantoro, Zulhadjri, H. Nur, Review of CIGS-based solar cells manufacturing by structural engineering, Sol. Energy 207 (2020) 1146–1157.
[29] Y.-C. Wang, T.-T. Wu, Y.-L. Chueh, A critical review on flexible Cu(In, Ga)Se2 (CIGS) solar cells, Mater. Chem. Phys. 234 (2019) 329–344.
[30] K.H. Ong, R. Agileswari, B. Maniscalco, P. Arnou, C.C. Kumar, J.W. Bowers, M. B. Marsadek, Review on substrate and molybdenum back contact in CIGS thin film solar cell, Int. J. Photo 2018 (2018) 9106269.
[31] L. Gouillart, A. Cattoni, W.-C. Chen, J. Goffard, L. Riekehr, J. Keller, M. Jubault, N. Naghavi, M. Edoff, S. Collin, Interface engineering of ultrathin Cu(In,Ga)Se2 solar cells on reflective back contacts, Prog. Photovolt.: Res. Appl. 29 (2021) 212–221.
[32] Y. Chen, X. Feng, M. Liu, J. Su, S. Shen, Towards efficient solar-to-hydrogen conversion: fundamentals and recent progress in copper-based chalcogenide photocathodes, Nanophotonics 5 (2016) 524–547.
[33] D. Yokoyama, T. Minegishi, K. Maeda, M. Katayama, J. Kubota, A. Yamada, M. Konagai, K. Domen, Photoelectrochemical water splitting using a Cu(In,Ga)Se2 thin film, Electrochem. Commun. 12 (2010) 851–853.
[34] T.J. Jacobsson, V. Fjällström, M. Edoff, T. Edvinsson, Sustainable solar hydrogen production: from photoelectrochemical cells to PV-electrolyzers and back again, Energy Environ. Sci. 7 (2014) 2056–2070.
[35] M.G. Mali, H. Yoon, B.N. Joshi, H. Park, S.S. Al-Deyab, D.C. Lim, S. Ahn, C. Nervi, S.S. Yoon, Enhanced photoelectrochemical solar water splitting using a platinum-decorated CIGS/CdS/ZnO photocathode, ACS Appl. Mater. Interfaces 7 (2015) 21619–21625.
[36] T. Klinkert, T. Hildebrandt, M. Jubault, F. Donsanti, J.-F. Guillemoles, N. Naghavi, Adaptation of the surface-near Ga content in co-evaporated Cu(In,Ga)Se_2 for CdS versus Zn(S,O)-based buffer layers, Thin Solid Films 582 (2015) 295–299.
[37] H. Liu, A. Zakhtser, A. Naitabdi, F. Rochet, F. Bournel, C. Salzemann, C. Petit, J.-J. Gallet, W. Jie, Operando near-ambient pressure X-ray photoelectron spectroscopy study of the CO oxidation reaction on the oxide/metal model catalyst ZnO/Pt(111), ACS Catal. 9 (2019) 10212–10225.
[38] A.D. Cicco, G. Aquilanti, M. Minicucci, E. Principi, N. Novello, A. Cognigni, L. Olivi, Novel XAFS capabilities at ELETTRA synchrotron light source, J. Phys.: Conf. Ser. 190 (2009), 012043.
[39] T. Klinkert, M. Jubault, F. Donsanti, D. Lincot, J.F. Guillemoles, Ga gradients in Cu (In,Ga)Se2: formation, characterization, and consequences, J. Renew. Sustain. Energy 6 (2014).
[40] H. Saïdi, C. Ben Alaya, M.F. Boujmil, B. Durand, J.L. Lazzari, M. Bouaïcha, Physical properties of electrodeposited CIGS films on crystalline silicon: Application for photovoltaic hetero-junction, Curr. Appl. Phys. 20 (2020) 29–36.

[41] S. Fazlikeshteli, X. Vendrell, J. Llorca, Low-temperature methane partial oxidation over Pd supported on CeO2: effect of the preparation method and precursors, Reactions 2 (2021) 30–42.
[42] J.-H. Kim, Z. Tian, M.-G. Kim, S.-J. Kwon, An X-ray absorption spectroscopic study of carbon monoxide-adsorbed Cu surface, Surf. Interface Anal. 46 (2014) 289–292.
[43] E.M. Erickson, M.S. Thorum, R. Vasić, N.S. Marinković, A.I. Frenkel, A.A. Gewirth, R.G. Nuzzo, In situ electrochemical X-ray absorption spectroscopy of oxygen reduction electrocatalysis with high oxygen flux, J. Am. Chem. Soc. 134 (2012) 197–200.
[44] J. Li, Y. Ma, G. Chen, J. Gong, X. Wang, Y. Kong, X. Ma, K. Wang, W. Li, C. Yang, X. Xiao, Effects of ammonia-induced surface modification of Cu(In,Ga)Se2 on high-efficiency Zn(O,S)-based Cu(In,Ga)Se2 solar cells, Sol. RRL 3 (2019) 1800254.
[45] J.-f Han, C. Liao, L.-m Cha, T. Jiang, H.-m Xie, K. Zhao, M.P. Besland, TEM and XPS studies on CdS/CIGS interfaces, J. Phys. Chem. Solids 75 (2014) 1279–1283.
[46] S. Béchu, M. Bouttemy, J.-F. Guillemoles, A. Etcheberry, The influence of relative humidity upon Cu(In,Ga)Se2 thin-film surface chemistry: an X-ray photoelectron spectroscopy study, Appl. Surf. Sci. 576 (2022).
[47] A. Loubat, S. Béchu, M. Bouttemy, J. Vigneron, D. Lincot, J.-F. Guillemoles, A. Etcheberry, Cu depletion on Cu(In,Ga)Se2 surfaces investigated by chemical engineering: an x-ray photoelectron spectroscopy approach, J. Vac. Sci. Technol. A 37 (2019).
[48] K.N. Kudin, B. Ozbas, H.C. Schniepp, R.K. Prud'homme, I.A. Aksay, R. Car, Raman spectra of graphite oxide and functionalized graphene sheets, Nano Lett. 8 (2008) 36–41.
[49] M. Yamamoto, Y. Sakurai, Y. Hosoi, H. Ishii, K. Kajikawa, Y. Ouchi, K. Seki, Softened CH stretching vibration of a long-chain n-alkane, n-C44H90, physisorbed on a Ag(111) surface: an infrared reflection absorption spectroscopic study, J. Phys. Chem. B 104 (2000) 7370–7376.
[50] M. Bär, S. Nishiwaki, L. Weinhardt, S. Pookpanratana, W.N. Shafarman, C. Heske, Electronic level alignment at the deeply buried absorber/Mo interface in chalcopyrite-based thin film solar cells, Appl. Phys. Lett. 93 (2008), 042110.
[51] X.-D. Chen, L. Chen, Q.-Q. Sun, P. Zhou, D.W. Zhang, Hybrid density functional theory study of Cu(In1−xGax)Se2 band structure for solar cell application, AIP Adv. 4 (2014), 087118.
[52] M. Prettre, C. Eichner, M. Perrin, The catalytic oxidation of methane to carbon monoxide and hydrogen, Trans. Faraday Soc. 42 (1946) 335b–339b.
[53] A.P.E. York, T. Xiao, M.L.H. Green, Brief overview of the partial oxidation of methane to synthesis gas, Top. Catal. 22 (2003) 345–358.